ELSEVIER

Journal of Power Sources 68 (1997) 338–343

JOURNAL OF POWER SOURCES

Performances of Li/Li_xCoO_2 cells in $LiAlCl_4 \cdot 3SO_2$ electrolyte

Chul Wan Park, Seung M. Oh *

Department of Chemical Technology, College of Engineering, Seoul National University, Seoul 151-742, South Korea

Received 20 September 1996; accepted 2 December 1996

Abstract

A nonaqueous inorganic electrolyte, $LiAlCl_4 \cdot 3SO_2$, was employed in an Li/Li_xCoO_2 rechargeable battery. In this medium, the Li_xCoO_2 cathodes reversibly intercalate and de-intercalate Li^+ ions at 3.90 and 3.92 V (versus Li/Li^+), respectively. Because of the high electrolyte conductivity (about 0.1 S cm^{-1} at 0–25 °C), the cell could be operated at a relatively high charge/discharge rate (*C*/1 rate) even at subambient temperature. Anode degradation could be alleviated by adding small amounts of $LiPF_6$ to the electrolyte. Cl_2 evolution at the end of the charging period (>4.07 V) was the major side reaction involved in the present cell system which has detrimental effects on the coulombic efficiency of the cells and on the cathodic reversibility. The observed cathode degradation seems to be caused by a Cl_2 attack on the cathode material. The Cl_2 generation was less significant at lower temperatures, such that a higher coulombic efficiency and better capacity retention could be achieved at lower temperatures even though the discharge voltages were slightly lower due to higher cell polarization. © 1997 Elsevier Science S.A.

Keywords: Lithium-ion rechargeable batteries; Lithium electrolyte, Cobalt, Cathode degradation

1. Introduction

Lithium-ion rechargeable batteries with organic electrolytes have achieved high energy density, excellent cycle life and sufficient safety characteristics. However, since liquid electrolytes have conductivities of about 10^{-2} S cm^{-1} at or under ambient temperature, their charge/discharge characteristics are not sufficiently good, particularly under high-rate cycling conditions. In general, these undesirable cell performances are caused by cell polarization induced by relatively high solution resistance of organic electrolytes at low temperatures. In addition, under a high-rate cell operation in resistive electrolytes, insufficient supply of Li^+ ions from a electrolyte to a electrode materials may give rise to irreversible phase formations and/or undesirable surface state variations in a electrode materials [1].

In Li/SO_2 primary cells, highly conductive SO_2 solvates of $LiAlCl_4$ are utilized as the electrolyte; they have been widely used by the military for moderate- to high-rate applications [2]. These cells have high energy density and show excellent low-temperature performances as a direct consequence of the highly conductive inorganic electrolytes. Recently, their secondary counterparts have been developed utilizing carbon cathodes with some successful performances [3,4]. These cells discharge at about 3 V, which is somewhat lower than the conventional lithium-ion batteries.

The $Li/LiAlCl_4 \cdot 3SO_2/Li_xCoO_2$ systems, where Li_xCoO_2 cathodes replace carbon electrodes in the Li/SO_2 rechargeable cells, can be projected as high-power secondary batteries that combine the merits of two battery systems; the high rate-capability with an inorganic electrolyte and high cell voltage (near to 4 V versus Li/Li^+) with Li_xCoO_2 cathodes. Reversible Li^+-ion intercalation/de-intercalation has already been reported for this battery system [5]. However, details on the low-temperature performance, cycling behavior, and cell degradation mechanism have not been fully exploited.

2. Experimental

2.1. Materials

The $LiAlCl_4 \cdot 3SO_2$ electrolyte was prepared by adding dry SO_2 gas (99.99%) into an equimolar mixture of LiCl (Aldrich, 99.9%) and $AlCl_3$ (Aldrich, 99.99%). During the SO_2 addition, the weight of mixture was monitored until the solvate number reached at 3. The solvate number was further confirmed by comparing the observed ionic conductivity with the pre-calibrated value. Since the electric conductivity of $LiAlCl_4 \cdot nSO_2$ electrolyte widely varies according to the sol-

* Corresponding author. Tel: 82-2-880-7074; Fax 82-2-888-1604, e-mail: seungoh@plaza.snu.ac.kr

PII S0378-7753(97)02518-4

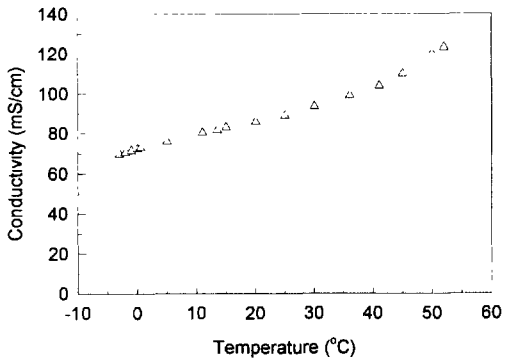

Fig. 1. Conductivity of the $LiAlCl_4 \cdot 3SO_2$ electrolyte as a function of temperature. The measurements were made with a conductivity meter (Orion 170) of which the cell constant was 1.5 cm^{-1}.

vate number n and measured temperature [3,4], it can serve as a sensible probe for the determination of solvate number. According to this study, when $n=3$ and $T=25$ °C, the conductivity was 90 ± 3 mS cm^{-1} (Fig. 1). For the preparation of high temperature (HT) Li_xCoO_2, a mixture of $LiOH \cdot H_2O$ and $CoCO_3 \cdot 6H_2O$ (molar ratio = 1.05:1.0) was dispersed in hexane and ball-milled for 24 h. The mixture was then calcined at 950 °C for 24 h with a heating and cooling rate of 1 °C min^{-1}. The X-ray diffraction results indicated that the powder products were highly crystalline with a layered-type (α-$NaFeO_2$) structure.

To prepare the composite cathodes, HT-Li_xCoO_2 powder was mixed with Vulcan XC-72 (Cabot) and Teflon binder with a weight ratio of 84:8:8. The doughs were then dispersed in isopropyl alcohol and spread on a piece of nickel exmet (long width dimension: 2 mm, short width dimension: 1 mm, area: 0.25 cm^2), followed by pressing and drying at 120 °C for 3 h. Cell performances were tested with a three-electrode cell, where a lithium foil (Cyprus Foote Mineral) was used as the anode and reference electrodes. A glass fiber sheet (Whatman) was used as the separator.

2.2. Instrumentations

The charge/discharge cycling was performed galvanostatically with a current density of 2 mA cm^{-2} ($C/1$ rate). The cut-off voltages for the discharge and charge limit were fixed at 3.35 and 4.1 V (versus Li/Li^+), respectively. A.c. impedance measurements were made over the frequency range of 0.005 Hz to 100 kHz using an EG&G PARC M173 potentiostat, M276 interface, and 5208 lock-in analyzer. Spectra were obtained at an open-circuit condition with an a.c. amplitude of 10 mV. Deconvolution of the complex impedance spectra was performed with an EQUIVCRT software. For the electrochemical voltage spectroscopy (EVS) measurements [6,7], an EG&G PARC M362 potentiostat and programmable voltage source were combined to control the applied voltage step, and the current was continuously monitored until it decayed to a pre-set threshold value ($I_{threshold}$ = 0.01 mA). The cell potential was increased stepwise by dV (= 10 mV).

3. Results and discussion

3.1. Electrolyte and cell performances

Ionic conductivity of $LiAlCl_4 \cdot 3SO_2$ electrolyte was measured from −10 to 50 °C (Fig. 1). The conductivity was fairly proportional to the measured temperature which ranged from 70–130 mS cm^{-1} in good agreement with the reported values [3,4,8,9]. Obviously, the conductivities are one order of magnitude higher than those observed in organic electrolytes.

Fig. 2 shows the EVS profile traced with a HT-Li_xCoO_2 composite cathode in an $LiAlCl_4 \cdot 3SO_2$ electrolyte. In the negative scanning direction, one current peak at 3.90 V (versus Li/Li^+) appears while two at 3.92 and >4.07 V in the reverse direction. The paired peaks near to 3.9 V are readily assigned to the currents associated with Li^+ intercalation/de-intercalation reaction since the same current peaks were observed in organic electrolytes [10]. The second anodic peak appeared at >4.07 V is assigned to the Cl_2 evolution by referencing the literatures [3,4]. As will be described in the later section, this undesirable reaction has harmful effects on the cell performances such as current efficiency and cathode reversibility. Even so, any solid evidence for this reaction, for instance a pressure build-up in the cells, cannot be provided in this study. This is believed to be due to the accompanying Cl_2 dissipation reactions as described below:

(i) Cl_2 generation on cathodes during the charging period

$$LiAlCl_4 \rightarrow AlCl_3 + \frac{1}{2}Cl_{2(dissolved)} + Li^+ + e^- \quad (1)$$

(ii) Cl_2 dissipation on Li anode

$$\frac{1}{2}Cl_{2(dissolved)} + Li_{(s)} \rightarrow LiCl_{(s)} \quad (2)$$

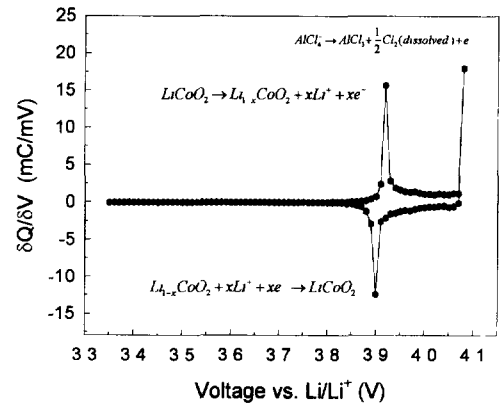

Fig. 2. Cathodic electrochemical voltage spectroscopy (EVS) profile traced with the $Li/LiAlCl_4 \cdot 3SO_2$/HT-Li_xCoO_2 cell at 25 °C. The voltage scale was referenced against the additional lithium electrode.

(iii) Cl_2 dissipation on composite cathode

$$\frac{y}{2}Cl_{2(dissolved)} + Li_xCoO_2 \rightarrow Li_{x-y}CoO_2 + yLiCl_{(s)} \quad (3)$$

(iv) $LiAlCl_4$ regeneration

$$LiCl_{(s)} + AlCl_3 \rightarrow LiAlCl_4 \quad (4)$$

As suggested in these equations, gaseous Cl_2 is first produced as a result of the electrochemical oxidation of $LiAlCl_4$ on the carbon surface of the composite cathode. Then, as-generated Cl_2 is dissolved into the electrolyte and diffused to the anode and cathode. The accompanying Cl_2 dissipation reactions on both electrodes produce LiCl, which further reacts with $AlCl_3$ to produce $LiAlCl_4$. A similar Cl_2 generation/dissipation reaction has been proposed by Foster et al. [3] and Schlaikjer and Jones [4] in Li/SO_2 secondary cells. In fact, the two cell systems differ in the cathode-active materials, such that it is hard at a first glance to believe that the Cl_2 evolution takes place in the present cells. However, since the composite cathodes used in this study also contain carbon particles, it is not difficult to assume this reaction being still prevailed in the present cells.

Fig. 3 shows two discharge capacity profiles where a distinction is made by the presence/absence of $LiPF_6$ in the electrolyte. Without $LiPF_6$, the discharge capacity steadily decreases to become half of the initial value after 30 cycles. We could also notice the lithium surface being covered with a porous layer after dissembling the cell. In general, reversible lithium deposition/dissolution in lithium secondary batteries cannot be fully accomplished. In many organic solvents, the lithium surface is passivated to form ionically conductive film and this surface layer is strongly related to the formation of dendritic lithium. Surface modification, particularly by including additives, may control the morphology of lithium deposits so as to suppress the dendritic growth. One such an effort is the addition of $LiPF_6$ in organic electrolytes. Kanamura et al. [11] have reported that hydrogen fluoride, generated by the reaction between $LiPF_6$ and trace amounts of water in organic electrolytes, can improve the reversibility of the lithium anode through the formation of a uniform, hemispherical passive layer on the lithium surface. In this study, the addition of small amounts (<5 mM) of $LiPF_6$ leads to a similar improvement in cell performances. As shown in Fig. 3, the capacity is retained at 80% of the initial value after 30 cycles when $LiPF_6$ is added. We could also visually recognize that the $LiPF_6$-treated lithium surface is much cleaner than the untreated one. In order to characterize the $LiPF_6$ effects, the resistance of the passive layers on the lithium surfaces were measured using a.c. impedance techniques and the results are compared in Table 1. As shown, the interfacial resistance values without $LiPF_6$ are larger in magnitude and further the increasing rate is faster than those of $LiPF_6$ treated. Undoubtedly, the higher interfacial resistance would give rise to appreciable cell polarization and concomitantly the charging capacity would fall down steadily.

As shown in Fig. 3, the discharge capacity steadily decreases even in the presence of $LiPF_6$, which manifests itself that other factors are involved in the cell degradation. We turned our attention to the cathode side and took a.c. impedance spectra on the cathode (Fig. 4). The resulting impedance parameters, deconvoluted with the equivalent circuits depicted in the inset, are listed in Table 2. In the fresh state where the cathode-active material is fully lithiated, Li^+ absorption is not so facilitated that the cathode acts as a blocking electrode for Li^+ ions. Thus, the equivalent circuit

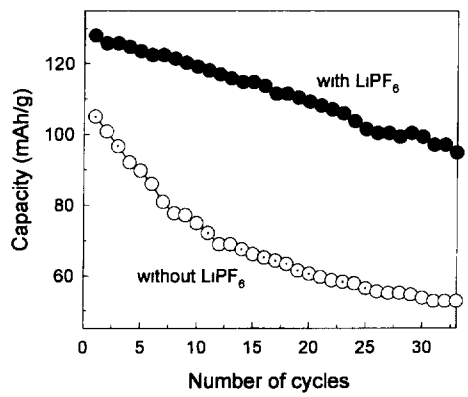

Fig. 3. Discharge capacities on cycling with/without $LiPF_6$ addition. The results were obtained at 25 °C and the $LiPF_6$ concentration was <5 mM.

Table 1
Resistances of the passivating layer on Li anode [a]

	with $LiPF_6$	without $LiPF_6$
Initial state (Ω)	5	8
After storage of 40 h (Ω)	12	35

[a] The numbers were obtained by a.c. impedance measurements with a cell configuration of Li/$LiAlCl_4 \cdot 3SO_2$/Li at 25 °C. The apparent electrode area was 1 cm^2 and the $LiPF_6$ concentration was <5 mM.

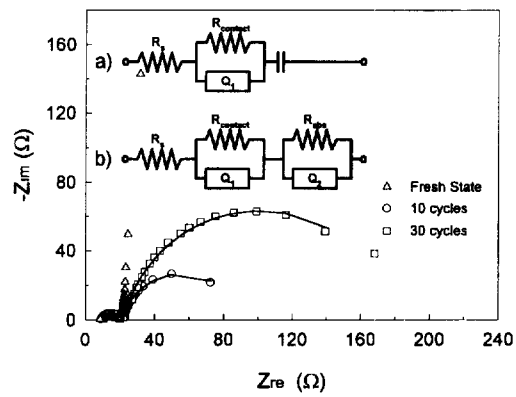

Fig. 4. Cathodic a.c. impedance spectra obtained with the Li/$LiAlCl_4 \cdot 3SO_2$, $LiPF_6$/HT-Li_xCoO_2 cells at 25 °C with repeated cycling. The equivalent circuit for the (a) fresh and (b) cycled cathodes were presented in the inset. The spectra were taken at the end of discharge reaction. An a.c. voltage was applied between the additional lithium reference electrode and the composite cathodes. The apparent electrode area was 0.25 cm^2 and the $LiPF_6$ concentration was <5 mM.

Table 2
Deconvoluted a.c. impedance parameters obtained with the spectra of Fig. 4

Number of cycles	R_s (Ω)	$R_{contact}$ (Ω)	Q_1^* (Ω^{-1}) [a]		R_{abs} (Ω)	Q_2^* (Ω^{-1}) [a]	
			Y_o	n		Y_o	n
Fresh	8.8	8.5	6.5×10^{-6}	0.87			
10	6.8	14.5	9.2×10^{-5}	0.59	68.0	1.5×10^{-2}	0.84
30	7.3	14.6	8.5×10^{-5}	0.58	159.0	1.4×10^{-2}	0.86

[a] Q is the circuit description code (CDC) representing the constant phase element (CPE). Representation of CPE in admittance is $Y(\omega)=Y_o\cdot(j\omega)^n$. The apparent cathode area was 0.25 cm^2. $T=25$°C

can be expressed as Fig. 4(a), where R_s indicates the solution resistance between the composite cathode and reference electrode, and $R_{contact}$ the contact resistance between Li_xCoO_2 and carbon particulates in the composite cathodes. The spectra taken after several cycles, however, show another semicircle in the lower frequency region. The best fitting of the latter spectra was achieved with the equivalent circuit, shown in Fig. 4(b), where the additional lower frequency semicircle has been assigned to a parallel combination of the constant phase element (CPE) and the resistances for Li^+ absorption [12,13]. As the Table illustrates, both $R_{contact}$ and R_{abs} values increase with repeated cycling but at a faster rate in the latter component. This results suggest that the capacity degradation observed in the $LiPF_6$ added cells (Fig. 3) is now deeply associated with the cathodes and the cell degrading reactions, whatever they are in nature, cause an increase in $R_{contact}$ and R_{abs} of the cathodes.

3.2. Low-temperature cell performances and cell degradation mechanism

Fig. 5 shows the first charge/discharge profiles obtained at three different temperatures, where two features are immediately apparent: (i) the discharge capacities decrease with decreasing temperature, and (ii) the difference between the discharging and charging voltages becomes wider at lower temperatures. These features can readily be explained on the basis of the cell polarizations which should also be temperature dependent; that is, higher electrolyte resistances and sluggish electrode reactions at lower temperatures lead to higher cell polarizations.

Table 3 lists the temperature-dependent coulombic efficiencies calculated from the charge and discharge capacity values obtained from the second cycle. As listed, the coulombic efficiencies decrease with increasing temperature. As described in the previous section, there is a side reaction in the charging process but no noticeable ones in the discharging process (Fig. 2). From this, the lower coulombic efficiencies at higher temperatures can be accounted for by the large extra charge consumption for Cl_2 generation at higher tempera-

Table 3
Coulombic efficiencies as a function of temperature and cycle numbers [a]

Temperature (°C)	Coulombic efficiency (%)			
	2nd cycle	10th cycle	20th cycle	30th cycle
0	98.1	97.3	97.3	97.1
12	94.4	95.6	95.4	93.7
25	89.8	88.5	85.3	83.3

[a] The coulombic efficiency was defined as the ratio of discharge capacity/charging capacity. The experimental conditions were the same as those for Fig. 5.

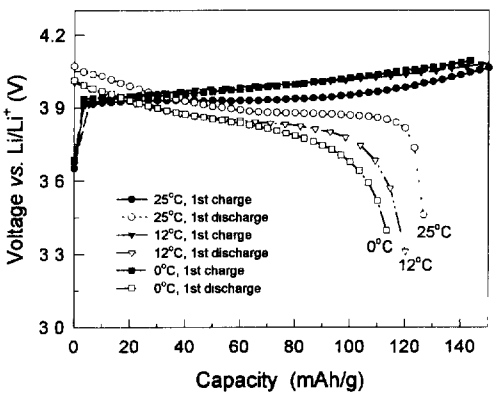

Fig. 5. The first charge/discharge profiles of the Li/$LiAlCl_4\cdot3SO_2$, $LiPF_6$/HT-Li_xCoO_2 cells at various temperatures. The voltage scale was referenced against the additional lithium electrode. Other experimental conditions were the same as those for Fig. 4.

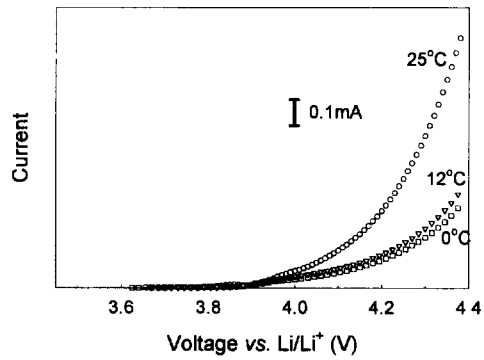

Fig. 6. Linear sweep voltammograms recorded with the composite carbon electrode (Vulcan XC-72:Teflon binder = 95:5 in weight ratio) at different temperatures. The anodic currents correspond to the Cl_2 evolution.

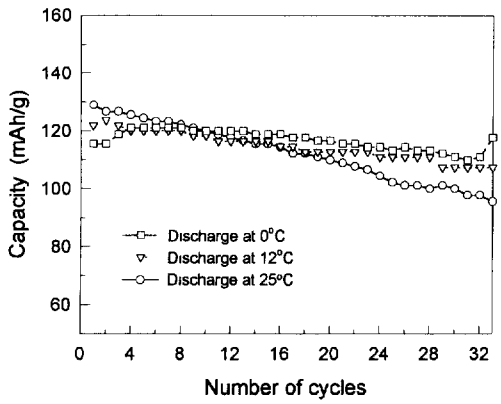

Fig. 7. Discharge capacity variations at three different temperatures. The experimental conditions were the same as those for Fig. 4.

tures. As a matter of fact, the Cl_2 formation is proportional to temperature as demonstrated in Fig. 6, where the linear sweep voltammograms traced with the composite carbon electrode at three different temperatures are reproduced.

Aside from the discussion on the temperature-dependent Cl_2 generation, the result in Fig. 6 provides an additional insight into the nature of reaction sites for Cl_2 generation. The voltammograms in Fig. 6 were recorded with a carbon electrode (without Li_xCoO_2) in $LiAlCl_4 \cdot 3SO_2$ medium. This observation illustrates that the Cl_2 evolution takes place mainly on the carbon surface rather than $Li_{1-x}CoO_2$ of the composite cathodes. This is reasonable if one takes into account the active surface area of the carbon additives which is much larger than that of the active materials.

Besides the coulombic efficiency, the discharge capacities are also temperature dependent as demonstrated in Fig. 7. Clearly, a better capacity retention is achieved at lower temperatures, illustrating that the cell degradation reactions are slowed down at lower temperatures. Although many lithium-ion batteries possess good energy density and cycle life, gradual capacity losses are inevitable in every cell. The capacity degradation comes from several sources such as phase transformations in electrode materials, variations in electrode surface properties and electrolyte decomposition due to electrode/electrolyte reactions. In the case of Li_xCoO_2, the reversible cell reactions are possible only in the range of $x = 0.5$–1.0 and if $x < 0.4$, there occurs a transformation to electrochemically inactive phases [14]. Combining this and another observation whereby inorganic electrolytes Li^+ ions are easily extracted from the Li_xCoO_2 lattice by the action of Cl_2 [15], it is believed that the Cl_2 attack on the cathode-active material (Eq. (3) in the previous section) is deeply involved in the cathode degradation in the present cell system. That is, at the later stage of the charging process where x approaches the lower end of the reversible range ($x = 0.5$), the Cl_2 evolution rate is sufficiently high since the cathodic potential is very positive. In this circumstance, if the Li^+ extraction reaction (Eq. (3)) indeed takes place, the Li^+ content in Li_xCoO_2 would further be decreased to below the lower limit of the reversible range, which causes a possible transformation to inactive phases. As a result of these serial reactions, the inactive components would keep growing with cycling, accompanied by a large increase in the lithium intercalation/de-intercalation resistance (R_{abs}).

4. Conclusions

We report here the cell performances of $Li/LiAlCl_4 \cdot 3SO_2/Li_xCoO_2$ rechargeable batteries. The following points summarize our findings. First of all, the inorganic electrolyte showed a reasonably high conductivity even at subambient temperatures and the Li_xCoO_2 cathodes successfully intercalated/de-intercalated Li^+ ions at about 3.9 V. The conventional Li/SO_2 secondary cells exhibit reasonable low-temperature performances but the cells discharge only at 3 V. The conventional lithium-ion batteries loaded with Li_xCoO_2 cathodes have higher cell voltage (about 4 V) but the low-temperature performance does not meet our target. The present cells combine the merits of two cell systems; the highly conductive electrolyte and the cathode materials that discharge at high voltage (near to 3.9 V). The anodic performances in the present cells were improved by adding small amounts of $LiPF_6$ into the electrolyte. The cathodic capacities steadily decreased due to Cl_2 attack on the cathode materials. The initial capacities were retained for longer cycling at lower temperatures since the Cl_2 formation was suppressed.

The present cell combination could be a possible candidate for high-power secondary batteries that can be operated at subambient temperatures for special applications. However, in order for the present cell system to be practical, the Cl_2 problem should be solved. To lessen the Cl_2 evolution, a deliberate selection and surface modification of carbon additives should be tried. Lowering the charging potential by reducing cell polarizations would be another pathway to overcome the Cl_2 problem.

Acknowledgements

The financial support by the Agency for Defence Development (Korea) is gratefully acknowledged. The authors wish to thank Professors Tak Kang and Hun-Joon Sohn, Seoul National University for their helpful discussions.

References

[1] G.G Amatucci, J.M Tarascon and L.C. Klein, *Solid State Ionics, 83* (1996) 167.
[2] F.C. Laman, J A.R. Stiles, K.J Shank and K. Brant, *J. Power Sources, 14* (1985) 201
[3] D L. Foster, H C Kuo, C.R Schlaikjer and A N. Dey, *J Electrochem Soc., 135* (1988) 2682.
[4] C R. Schlaikjer and M.D. Jones, *US Patent No. 5 145 755* (1992).

[5] J. Dreher, B Haas and G Hambitzer, *J. Power Sources, 43/44* (1993) 583
[6] A.H. Thompson, *J Electrochem Soc., 126* (1979) 608
[7] A.H Thompson, *Phys Rev., 40* (1978) 1511.
[8] A.N. Dey, H C Kuo, D. Foster, C. Schlaikjer and M. Kallianidis, *Proc. 32nd Int Power Sources Symp., Cherry Hill, NJ, USA, June, 1986*, p 176
[9] T C. Murphy, D M. Cason-Smith, S.D. James and P.H. Smith, *Proc. 34th Int. Power Sources Symp., 1990, Cherry Hill, NJ, USA, June*, pp. 172–180.
[10] I. Uchida and H. Sato, *J. Electrochem. Soc., 142* (1995) L139.
[11] K. Kanamura, H Tamura and Z Takehara *J Electrochem. Soc., 142* (1995) 340.
[12] D H. Jang, Y J. Shin and S M. Oh, *J Electrochem Soc., 143* (1996) 2204.
[13] J.R Macdonald, *Impedance Spectroscopy Emphasizing Solid Materials and System*, Wiley, New York, 1987
[14] T. Ohzuku and A. Ueda, *J Electrochem Soc., 141* (1994) 2972
[15] R. Cupta and A. Manthiram, *J. Solid State Chem., 121* (1996) 483.